A Polymer Blend Electrolyte Based on CS with Enhanced Ion Transport and Electrochemical Properties for Electrical Double Layer Capacitor Applications

Shujahadeen B. Aziz [1,2,*], Elham M. A. Dannoun [3], Muhamad H. Hamsan [4], Hewa O. Ghareeb [5], Muaffaq M. Nofal [6], Wrya O. Karim [5], Ahmad S. F. M. Asnawi [7], Jihad M. Hadi [8] and Mohd Fakhrul Zamani Abdul Kadir [4]

[1] Hameed Majid Advanced Polymeric Materials Research Lab., Department of Physics, College of Science, University of Sulaimani, Qlyasan Street, Sulaimani 46001, Iraq
[2] Department of Civil Engineering, College of Engineering, Komar University of Science and Technology, Sulaimani 46001, Iraq
[3] General Science Department, Woman Campus, Prince Sultan University, P.O. Box 66833, Riyadh 11586, Saudi Arabia; elhamdannoun1977@gmail.com
[4] Centre for Foundation Studies in Science, University of Malaya, Kuala Lumpur 50603, Malaysia; hafizhamsan93@gmail.com (M.H.H.); mfzkadir@um.edu.my (M.F.Z.A.K.)
[5] Department of Chemistry, College of Science, University of Sulaimani, Qlyasan Street, Sulaimani 46001, Iraq; hewa.ghareeb@univsul.edu.iq (H.O.G.); wrya.karim@univsul.edu.iq (W.O.K.)
[6] Department of Mathematics and General Sciences, Prince Sultan University, P.O. Box 66833, Riyadh 11586, Saudi Arabia; muaffaqnofal@gmail.com
[7] Chemical Engineering Section, Universiti Kuala Lumpur Malaysian Institute of Chemical & Bioengineering Technology (UniKL MICET), Alor Gajah, Malacca 78000, Malaysia; asyafiq.asnawi@s.unikl.edu.my
[8] Department of Medical Laboratory of Science, College of Health Sciences, University of Human Development, Sulaimani 46001, Iraq; jihad.chemist@gmail.com
* Correspondence: shujahadeenaziz@gmail.com

Abstract: The fabrication of energy storage EDLC in this work is achieved with the implementation of a conducting chitosan–methylcellulose–NH_4NO_3–glycerol polymer electrolyte system. The simple solution cast method has been used to prepare the electrolyte. The impedance of the samples was fitted with equivalent circuits to design the circuit diagram. The parameters associated with ion transport are well studied at various plasticizer concentrations. The FTIR investigation has been done on the films to detect the interaction that occurs among plasticizer and polymer electrolyte. To get more insights into ion transport parameters, the FTIR was deconvoluted. The transport properties achieved from both impedance and FTIR are discussed in detail. It was discovered that the transport parameter findings are in good agreement with both impedance and FTIR studies. A sample with high transport properties was characterized for ion dominancy and stability through the TNM and LSV investigations. The dominancy of ions in the electrolyte verified as the t_{ion} of the electrolyte is established to be 0.933 whereas it is potentially stable up to 1.87 V. The rechargeability of the EDLC is steady up to 500 cycles. The internal resistance, energy density, and power density of the EDLC at the 1st cycle are 53 ohms, 6.97 Wh/kg, and 1941 W/kg, respectively.

Keywords: polymer blend; plasticizer; ion transport; EEC modeling; FTIR deconvolution; TNM and LSV study; EDLC device

1. Introduction

In the past few years, researchers have been deeply concerned about global issues regarding sustainable energy sources that are safe for the environment. The most prominent electrolyte used in batteries and supercapacitor industries is an electrolyte in the liquid form. A liquid electrolyte (LE) provides high ionic conductivity due to its low bulk resistance but has drawbacks like leakage of harmful gases or corrosive liquid [1]. Researchers are

attracted to study solid polymer electrolytes (SPEs). They are easier to handle due to their free-standing properties compared to LEs. Rapid technology development is needed in this era due to massive commercial demands on various electrical devices with different shapes and sizes. These demands can be solved with the implementation of SPEs [2]. Several advantages of SPEs include them being lightweight, of excellent thermal stability, high flexibility, cheap, and easy handling [3,4].

Plastic production worldwide has been boosted from ~2 million tons in 1950 to 8.3 billion tons in 2015. This is approximately an increase of 76% and results in increasing waste production. This plastic waste is in the environment, landfills, and oceans [5]. This is the main reason that biopolymers are studied in order to find alternatives to current non-biodegradable polymers. The most commonly studied marine biopolymer is chitosan (CS). CS can be a good ionic conductor due to its chemical structure (existence of OH and NH2) [6]. Methylcellulose (MC) is another biopolymer with great potential to be used in polymer electrolyte applications. MC is extracted when alkali-based cellulose is treated with methyl chloride. Its basic structural units are joined by β-(1→4) glycosidic bond [7,8]. Polymer blend, a method used in this work, is a straightforward process where two or more polymers form a superior material [9]. This is because the functional groups of each polymer interact with each other and provide more pathways for ions. CS and MC possess functional groups with lone pair electrons which are beneficial in ionic transportations.

A lot of ionic sources are available for SPE applications such as sodium, lithium, magnesium, potassium, silver, copper, and ammonium salts. This work is focused on the use of ammonium salts to fabricated protonic (H^+) energy devices. H^+ can be obtained not only from ammonium salts but also from inorganic acids like sulfuric acid (H_2SO_4) and phosphoric acid (H_3PO_4). Reports on these acids show a chemical degradation which is not good for energy device applications [10,11]. Ammonium nitrate (NH_4NO_3) is chosen in this work owing to its stumpy lattice energy of 648.9 kJ mol^{-1}. This value can be considered low compared to other ammonium salts, e.g., for ammonium acetate ($NH_4CH_3CO_2$), ammonium sulfate (($NH_4)_2SO_4$, and ammonium phosphate (($NH_4)_3PO_4$), the values are 703.1, 1754.7, and 3334.0 kJ mol^{-1}, respectively. In addition, lattice energy for ammonium bromide (NH_4Br), ammonium chloride (NH_4Cl) and ammonium fluoride (NH_4F) is 682.0, 708.0 and 834.0 kJ mol^{-1}, respectively [12,13]. A low lattice energy salt provides more free ions and all of these free ions can thus contribute to the energy storage process of the energy devices.

The process of energy storage for an electrochemical double-layer capacitor (EDLC) involves a non-Faradaic reaction which means that ions build a charge double-layer on the carbon-based electrodes [14]. It has been reported that EDLC has higher power density and easier fabrication methods compared to Faradaic capacitor or pseudocapacitor [15–17]. Activated carbon is the most commonly used active material in the electrodes of an EDLC [18–20]. Various activated carbons have been synthesized from different sources such as nori-based [21], tofu-based [22], dimocarpus longan-based [23], coconut shell-based [24], and many more. Unique properties of activated carbon such as excellent electron conductivity, reasonable price, easy handling, and good chemical stability, plus high surface area mark it a choice for EDLC applications [25]. In this effort, CS is blended with MC to form a polymer matrix. Ions are provided by the addition of NH_4NO_3 and glycerol. The electrolyte with the best performance will be chosen to be used in the EDLC fabrication.

2. Experimental Methods

2.1. Electrolyte Preparation

The preparation of polymer electrolytes was performed from the components of MC (4000 cP), CS (MW 310,000–375,000 g/mol), and low MW glycerol plasticizer. In a separate flask, CS:MC polymer blends were prepared by dissolving 30 wt.% MC and 70 wt.% of CS in 40 mL of 1% acetic acid at ambient temperature for about 3 h. The two solutions were then combined and stirred for further 2 h in order to obtain a homogeneous solution. To this

solution, 40 wt.% of NH_4NO_3 was added. Plasticization of the resulting CS:MC polymer blend solutions was performed by adding different quantities of 14, 28, and 42 wt.% glycerol. The obtained samples were denoted as MCCSNH1, MCCSNH2, and MCCSNH3, correspondingly. The contents of these samples were poured into the plastic petri dishes to cast the fabricated films, which were subsequently dried at ambient temperature. Prior to characterizations, the films were further dried using silica gel desiccant.

2.2. Characterization Techniques

2.2.1. FTIR and EIS Analyses

HIOKI 3531 Z Hi-tester was implemented to gain the impedance spectra of all samples over a frequency range f = 50 Hz–1000 kHz. Small pieces of 2 cm in diameter were cut from the films to prepare discs, which were placed between the two stainless steel (SS) electrodes underneath a spring pressure.

Moreover, Fourier transform infrared (FTIR) spectroscopy analysis was also carried out to investigate the interaction and complexation among the polymers, salt, and plasticizer. The FTIR analysis in this work was employed using a Spotlight 400 Perkin–Elmer spectrometer with 1-cm^{-1} resolution in the range of 500–4000 cm^{-1}. To further support the ionic conductivity studies, the ionic transport parameters; number density (n), ionic mobility (μ), and diffusion coefficient (D) based on the percentage of free ions were identified. The deconvolution method via the Gaussian–Lorentzian function was used to extract overlapping peaks as well as to correct the baseline of the curves.

2.2.2. Transference Number Analysis (TNM)

Transference number analysis (TNM) was conducted at a working voltage of 0.20 V using a V&A Instrument DP3003 digital DC power supply. The data were used to prove the involvement of ions in the entire conductivity. The electrolyte was sandwiched in between stainless steel (SS) electrodes. The summation of electronic (t_e) and ionic (t_i) transference number is equal to 1, where both values can be acquired from the subsequent equation:

$$t_i = \frac{I_i - I_{ss}}{I_i} \tag{1}$$

where I_{ss} and I_i are the steady-state current and initial current, respectively. The circuit for TNM structure is shown in Figure 1.
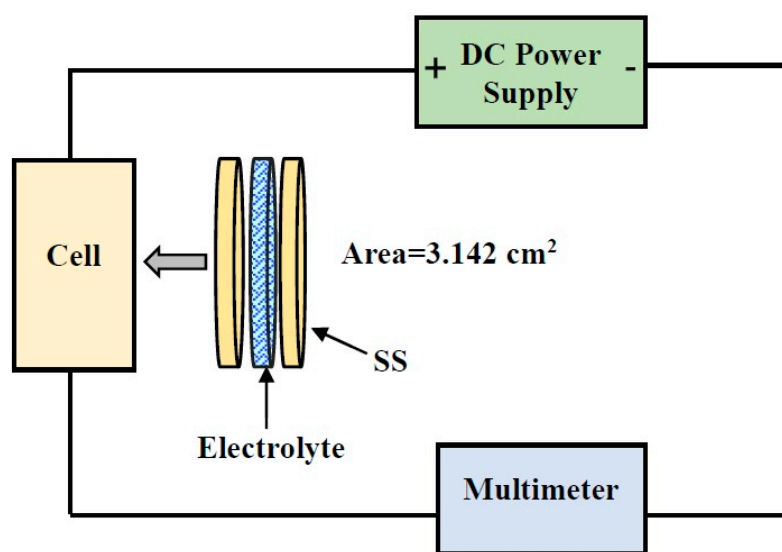

Figure 1. Circuit setup for Transference Number Analysis (TNM) measurement.

2.2.3. Linear Sweep Voltammetry (LSV)

The LSV analysis was performed using a Digi-IVY DY2300 potentiostat at a 0.02 V/s scan rate. The highest conducting sample was mounted in a Teflon holder with SS electrodes.

2.2.4. Steps to Fabricate EDLC and Their Characterization

Mixing and pulverization of 0.25 g of carbon black (CB) and 3.25 g of activated carbon (AC) powders were carried out using a planetary ball miller (XQM-0.4) at a rotation speed of 50 rpm for 15 min. Meanwhile, polyvinylidene fluoride (PVDF) as a binder was stirred in 15 mL of N-methyl pyrrolidone (NMP) solvent. Dissolution of the AC-CB powder mixture in the NMP-PVDF solution resulted in the formation of a thick black solution, which then varnished on an Al-foil using a doctor blade. After oven drying of the coated foil at 60 °C, the dried electrodes were cut into circular samples with area of 2.01 cm^2. The prime conducting electrolyte was situated between two carbon electrode CR2032 coin-type cells. As shown in Figure 2, these coin cells of EDLC were positioned in Teflon holders for further examination. The charge-discharge for the EDLC was measured using a Neware battery test system (current density = 0.5 mA/cm^2). The equations below are allowed calculating each specific capacitance (C), equivalent series resistance (ESR), efficiency, energy density (E), and power density (P) of the EDLC.

$$C = \frac{i}{xm} \tag{2}$$

$$ESR = \frac{V_d}{i} \tag{3}$$

$$efficiency = \frac{t_{dis}}{t_{cha}} \times 100\% \tag{4}$$

$$E = \frac{CV}{2} \tag{5}$$

$$P = \frac{V^2}{4mESR} \tag{6}$$

where i is the current apply, x the slope of discharge part, V_d is the drop voltage and m stands for the mass of activate material used. The times for discharge and charge parts are given as t_{dis} and t_{cha}, respectively.
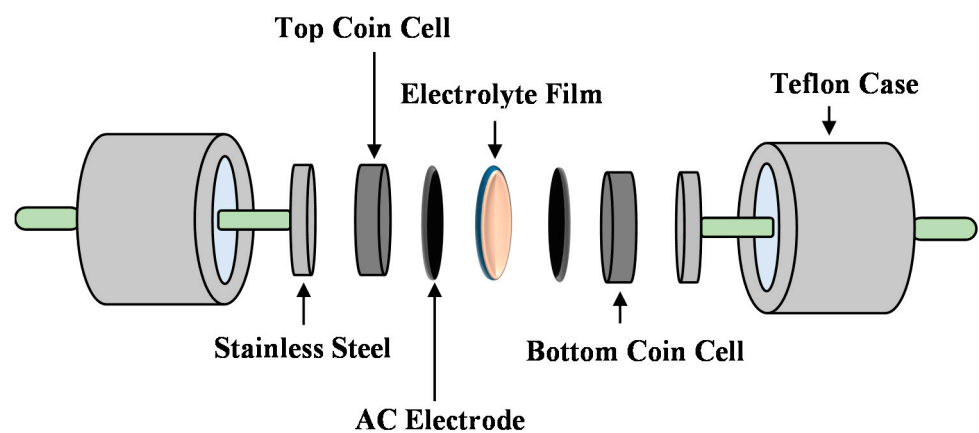

Figure 2. Illustration of the fabricated electrochemical double-layer capacitor (EDLC).

3. Results and Discussion

3.1. Impedance Study

PEs as part of an innovative class of materials are widely applied in devices [26]. Many investigational studies have confirmed the importance of adding low molecular weight plasticizers into the PEs for enhancing ion migration [27]. A significant role of impedance spectroscopy is the investigation of the electrical properties of a large variety of electrolyte materials and the electrode–electrolyte interfaces [28–30]. The impedance plots for the CS:MC:NH$_4$NO$_3$:glycerol system are depicted in Figure 3A–C. When the circuit composed of a capacitor and a resistor in parallel, the ideal impedance spectra should be a standard semicircle having a diameter-matched with the real axis. The absence of the high-frequency semicircular region indicates that the ions are primarily responsible for the conduction [31–33]. However, the presence of the spike at the low-frequency region results from the electric double-layer capacitance at the blocking electrodes [34–37]. As obviously seen in Figure 3A–C, the absence of the semicircles at the high-frequency region is owed to the use of the plasticizer [38]. This relation below is employed to calculate the impedance of CPE (Z_{CPE}) [39,40]:

$$Z_{CPE} = \frac{1}{C\omega^p}\left[\cos\left(\frac{\pi p}{2}\right) - i\sin\left(\frac{\pi p}{2}\right)\right] \tag{7}$$

where C, ω and p stand for the CPE capacitance, the angular frequency and the deviation measure of the plot from the axis, respectively. The CPE is connected in series with the R_b of the electrolytes and their EIS signals only display the spike [41]. The impedance can be mathematically represented as follows [42]:

$$Z_r = \frac{\cos\left(\frac{\pi p}{2}\right)}{C\omega^p} + R_b \tag{8}$$

$$Z_i = \frac{\sin\left(\frac{\pi p}{2}\right)}{C\omega^p} \tag{9}$$

These equations are also used in the fitting parameters (CPE1 and CPE2) and determined the R_b values precisely. The resulting R_b values and CPE values for the CMNG1, CMNG2, and CMNG3 electrolytes are listed in Table 1. The high values of CPE2 with the addition of glycerol can be explained on the basis of increasing the number of ions in the electrolytes. This results in an increase in the accelerating electrode polarization; thereby, an increase in the capacitance value at low frequency [43]. The addition of glycerol as a plasticizer enhances salt dissociation and hence increases ion mobility [44,45].

From Equation (10), the ionic conductivity (σ) can be calculated as the measure of the electrical properties of the electrolytes. The calculation also comprises R_b, t, and A values as charge resistance, thickness, and surface area, respectively. From Table 1, the conductivity values for the electrolytes are expressed by:

$$\sigma = \frac{t}{A \times R_b} \tag{10}$$

Commonly the σ_{dc} can be stated as follows [46]:

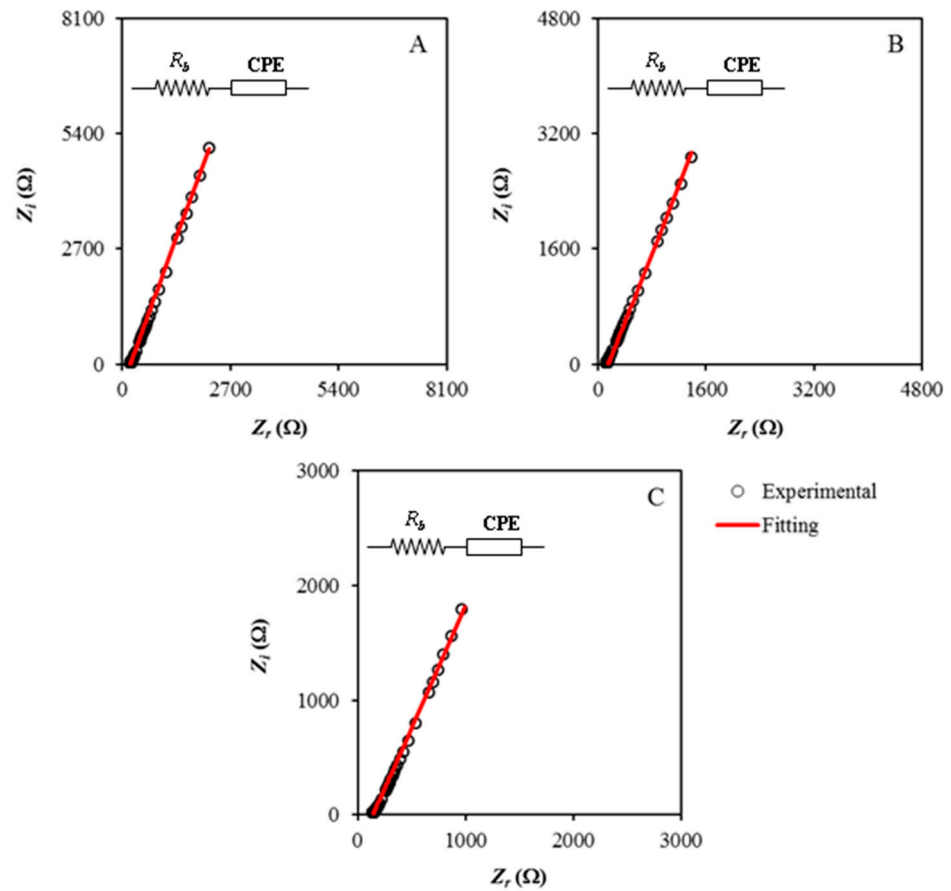$$\sigma_{dc} = \Sigma q\, n\, \mu \tag{11}$$

Figure 3. Nyquist plots of the electrolytes of (**A**) CMNG1, (**B**) CMNG2 and (**C**) CMNG3, respectively, at room temperature. The inset figure is the suitable electrical equivalent circuit.

Table 1. Room temperature ionic conductivity and circuit elements for the plasticized polymer electrolytes (PPEs).

Electrolyte	R_b (Ohm)	Conductivity (S cm^{-1})
CMNG1	200	6.97×10^{-5}
CMNG2	150	1.16×10^{-4}
CMNG3	140	1.31×10^{-4}

Previous investigations established that the H$^+$ ion released by ammonium ion is considered as the charge carrier species in such polymer/ammonium salt systems [47]. The extra plasticizer amended the number of charge carriers (n) through further salt dissociation and increase mobility (μ) by providing huge amorphous phases. Some equations can be applied to calculate the transport parameters such as diffusion coefficient (D), mobility (μ), and number density (n) of ions from impedance data possessing only a spike [48]. Beginning with the calculation of the D of ionic species, the following equation is employed:

$$D = D_\circ \exp\left\{ -0.0297[\ln D_\circ]^2 - 1.4348 \ln D_\circ - 14.504 \right\} \tag{12}$$

$$D_\circ = \left(\frac{4k^2 l^2}{R_b{}^4 \omega_{\min}{}^3} \right) \tag{13}$$

where l is the electrolyte thickness, ω_{min} is the angular frequency at the minimum Z_i value.

The mobility (μ) of the ionic species is determined from Equation (14),

$$\mu = \left(\frac{eD}{K_b T}\right) \tag{14}$$

where T is the absolute temperature and k_b is the Boltzmann constant.

Since DC conductivity of ions is obtainable from Equation (10), the density of ion carriers (n) can be determined from Equation (11). In Table 2, the parameters associated with the ion transport for all the systems are listed. There is a clear trend of increasing both values of D and μ with increasing glycerol quantity from 14 to 42 wt.%. These correlations are related to the chain flexibility enrichment in the presence of glycerol. The same trend of increasing n with increasing glycerol quantity is observed. All these, in turn, result in an increase in conductivity. A possible explanation of this is the role of glycerol molecules in enhancing the salt dissociation, thereby raising the number density of ion carriers [48]. In addition, the attractive forces between the anions and cations of the salt are greatly lowered [49]. Consequently, a higher number of NH_4^+ ions (n_i) is created by NH_4NO_3 into the polymer.

Table 2. The values of D, μ, and n at room temperature.

Electrolyte	n (cm^{-3})	μ (cm^{2}V^{-1}s^{-1})	D (cm^{2}s^{-1})	p (rad)	CPE * (F)
CMNG1	2.02×10^{21}	2.15×10^{-7}	5.53×10^{-9}	1.20	2.29×10^{-6}
CMNG2	2.73×10^{21}	2.65×10^{-7}	6.81×10^{-9}	1.17	4.35×10^{-6}
CMNG3	3.02×10^{21}	2.71×10^{-7}	6.97×10^{-9}	1.13	8.00×10^{-6}

* CPE: constant phase element.

3.2. FTIR Results

Figure 4 shows the FTIR spectra of the electrolytes at a wavenumber of 550–4000 cm^{-1}. The bands due to -OH stretching and -OH bending can be found at (i) 3700–3150 cm^{-1} in a broad peak form and (iv) 1250–1500 cm^{-1} in a sharp peak form, respectively which caused by the addition of glycerol into the system [50,51]. Numerous peaks are observed in-band region (iv) where the one centered at 1332 cm^{-1} came from -OH bending. In addition, the observed peak ascribed to the NH_4^+ asymmetry elucidates a high tendency of the NH_4^+ distortion to release H$^+$ ions [52]. Furthermore, the -CH symmetrical stretching and -CH asymmetrical stretching are found at the band region of (ii) 3050 to 2850c m^{-1} [53,54]. It is noticed that the intensity of the -CH bands is increased as the concentration of glycerol increases which signified the complex development between the glycerol and CS-MC-NH_4NO_3 [55]. The location carboxamide and amine band for the electrolytes are located at (iii) 1750–1520 cm^{-1} where a slight shift is observed when the concentration of glycerol increases. The shift shows the effect of glycerol concentration to provide more ions for the interaction with the oxygen and nitrogen atoms in the polymer blend [56]. Aziz et al. [57] and Shukur et al. [58] also reported a similar range of carboxamide and amine bands for their electrolyte systems. Lastly, the sharp peak located at (v) 900–1200 cm^{-1} possibly belongs to the C-O stretching which is comparable to the previous work reported by Mejenom et al. [59] and Poy et al. [60]. As the concentration of glycerol is increased, this band peak becomes sharper and causes a small shoulder peak to appear which also describes the interaction between the CS-MC-NH_4NO_3 and glycerol.
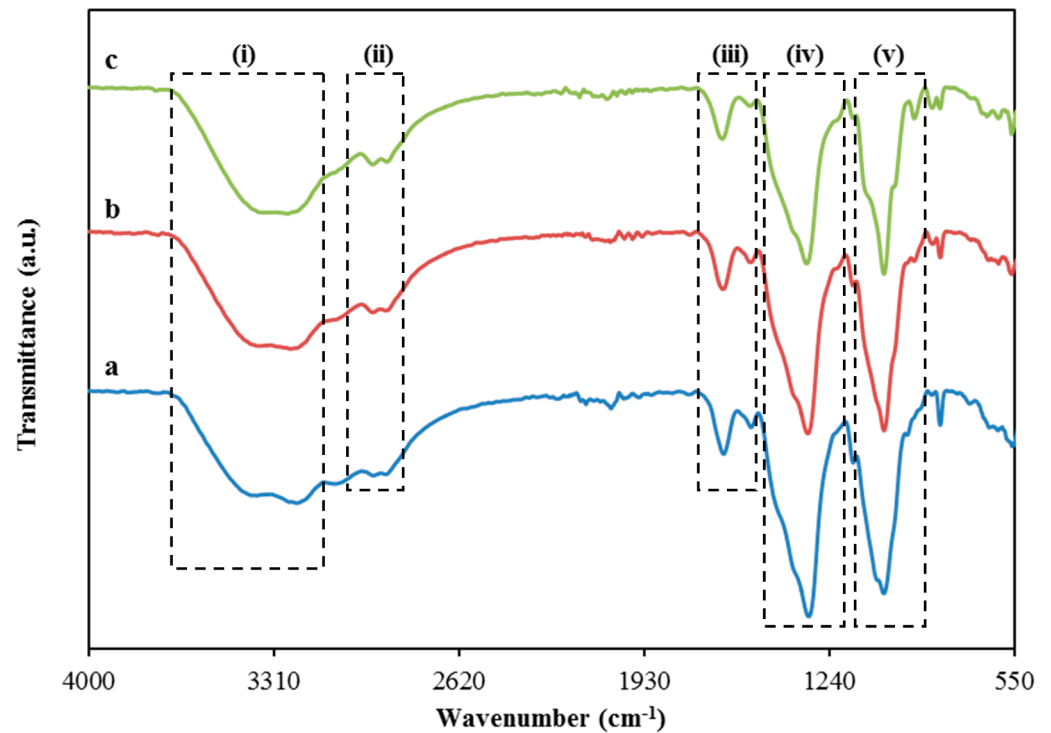
Figure 4. Fourier transform infrared spectroscopy (FTIR) spectra for (**a**) CMNG1, (**b**) CMNG2 and (**c**) CMNG3.

The FTIR deconvolution analysis is employed to support the ionic conductivity results where it also provides several advantageous properties such as resolving the overlapping peaks, removing noise and fringes from the spectrum, and inspecting the interconnection among deconvolution parameters [61]. Based on this approach, the deconvolution FTIR spectra can provide the fraction of conducting ions. The deconvolution possibility of FTIR spectra allowed one to isolate the existing peaks as well as alter both intensity and wavenumber as highlighted by Ramelli et al. [62]. Thus, the involvement of H^+ in charge carriers can be verified. The opted band region for the deconvolution purpose was from 1250 to 1500 cm^{-1}, as shown in Figure 5. This is payable to the evident interaction as before clarified in the FTIR analysis. In the same band region, the use of NH_4NO_3 led to shift the bands within the range of 1200–1500 cm^{-1}, as reported by Kamarudin and Isa [63] and Hafiza and Isa [64]. Thus, this approach is intended to isolate the free and ion pairs appropriately. The free ions correspond to the free mobile ions like H^+ while the ion pairs correspond to the ions of NH_4^+ or NO_3^- [65–67]. With the help of the deconvoluted FTIR spectra shown in Figure 5, the percentage of free ions can be quantified using the following equation:

$$\text{Free ions \%} = \frac{\text{Area of free ions peak}}{\text{Total area (free ions peak + ions pair peak)}} \times 100 \tag{15}$$
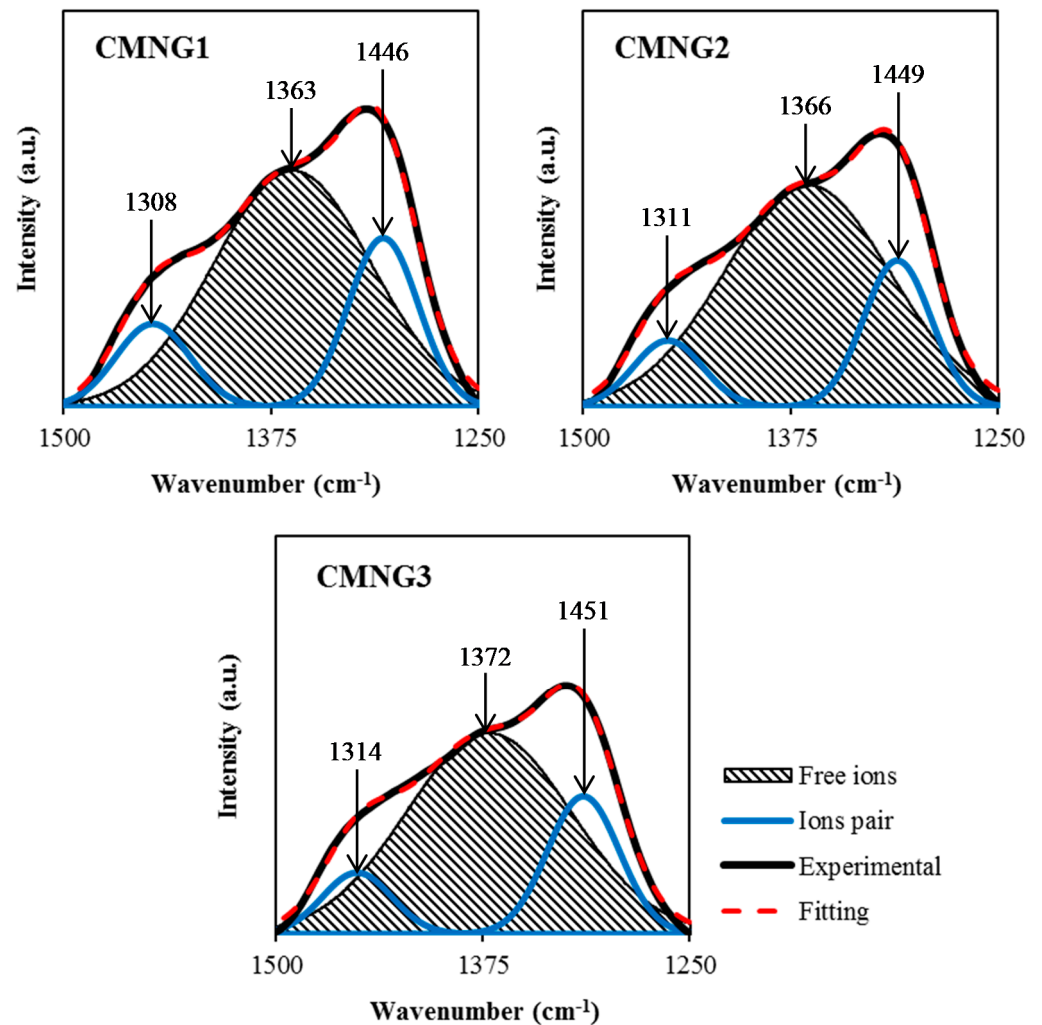
Figure 5. Deconvolution of FTIR spectra at 1250–1500 cm^{-1}.

The percentage of free ions obtained by CMNG1 is 67.5%, which then significantly increased to 71.7% with 28 wt.% of glycerol. However, a slight decrease of the free ions percentage to 70.2% is observed when the concentration of glycerol is increased to 42 wt.%. This is generally explained that the percentage of free ions is influenced by the concentration of glycerol in the system which is highly correlated to the trend of the ionic conductivity. The increase of H$^+$ ions that dissociated from NH$_4^+$ could also be a factor for the increment of ionic conductivity. Aniskari et al. [68] also reported the highest conducting electrolyte also had the highest percentage of free ions. By employing the percentage of free ions for each electrolyte, the transport parameters of number density (n), ionic mobility (μ), and diffusion coefficient (D), can be calculated using the Equations (16)–(18), where N_A is Avogadro's constant, M represents the number of moles of glycerol, and e is the elementary charge. V_{Total} is the total volume of the polymer electrolytes.

$$n = \frac{M \times N_A}{V_{Total}} \times (free\ ion\ \%) \tag{16}$$

$$\mu = \frac{\sigma}{ne} \tag{17}$$

$$D = \frac{\mu kT}{e} \tag{18}$$

The calculated transport parameters of the electrolytes are listed in Table 3 using FTIR routine. It can be observed that the trend of number density is followed the ionic conductivity pattern as in Table 1. The dissociation of H^+ ions assists to facilitate the coordination of the H^+ ions in the electrolyte system which leads to the enhancement of ionic conductivity value [69,70]. This can be further proved through the trend of μ and D. The flexibility and the segmental wave of the polymer chains in the system also predisposed the transport properties as well as the ionic conductivity [71]. However, the improvement of transport properties was observed when glycerol concentration reached 42 wt.% which is due to the enhancement of the chain flexibility that leads to the concentration increment of H^+ carriers, and thus increases the ionic conductivity of the electrolyte.

Table 3. Transport parameters values of the electrolytes.

Electrolyte	n (cm^{-3})	μ $(cm^2V^{-1}s^{-1})$	D (cm^2s^{-1})
CMNG1	4.90×10^{22}	1.02×10^{-8}	2.67×10^{-10}
CMNG2	6.31×10^{22}	1.11×10^{-8}	2.87×10^{-10}
CMNG3	6.80×10^{22}	1.14×10^{-8}	2.98×10^{-10}

3.3. Transference Number Study

The transfer of electrons and ions in an electrolyte provides conductivity. In order to determine the primary charge carrier, transference number (TNM) was evaluated at an applied voltage of 0.2 V. Figure 6 depicts polarization of the highest conductivity for the $CS:MC:NH_4NO_3$:glycerol system. It is obvious that at the beginning of the polarization process, the conduction of ions and electrons results in a significant current of 1.5 µA. As already mentioned, the evaluation is based on the SS electrode, owing to blocking the ions and permitting the electrons to pass. Therefore, as the time increases, the current minimizes up to a plateau at 0.1 µA. This steady-state current indicates the occurrence of a polarization process of the electrolyte. Thus, cations and anions are adsorbed at the negative electrode and the positive electrode, respectively [72,73]. At this stage, the current is only carried by electrons. The t_e value of 0.07 and the t_i value of 0.93 were obtained. Since t_i is higher than t_e, the dominant charge carriers of $CS:MC:NH_4NO_3$:glycerol electrolyte are the ions [74]. The accumulation of these ions on the surface electrodes allows EDLC applications. For the ammonium salt-based SPE reported by Vijaya et al. [75], the t_i values were in the range of 0.90 to 0.99. Samsi et al. [76] obtained the t_i value of 0.916 for cellulose acetate (75 wt.%)-NH_4I (25 wt.%) system. In another work, the ions are also dominated (i.e., 0.85 out of 1) in ammonium based-poly(ethyl methacrylate) system [77]. Alia et al. [78] revealed the t_i value of 0.905 for SPE of proton-based biopolymer with polycarbonate electrolyte as the plasticizer and zinc sulfate as the filler.

3.4. LSV Study

EDLC is known as a high cycle supercapacitor, thus it is crucial to investigate the working voltage range, frequently referred to as potential stability [79]. The study employed LSV, facilitated by SS electrodes, to identify the potential stability of every polymer electrolyte, and Figure 7 illustrates a normal LSV graph for the highest conducting $CS:MC:NH_4NO_3$:glycerol blend electrolyte. The finding indicates that, from the EDLC application viewpoint [80], the potential stability is in the satisfactory working voltage range of 1.87 V. According to Monisha et al. [81], the threshold voltage is that the current passes through the cells. The potential stability obtained for this work is comparable to other reports with ammonium salts as the ionic provider. A complexation of ethylene carbonate, NH_4NO_3, and CS yield potential stability of 1.8 V [82]. A system of $MC:NH_4Br$ is reported to decompose beyond 1.53 V [19]. In another report, poly (ε-caprolactone) (PCL)-based polymer electrolytes are stable up to 1.4 V as ammonium thiocyanate is added [83].
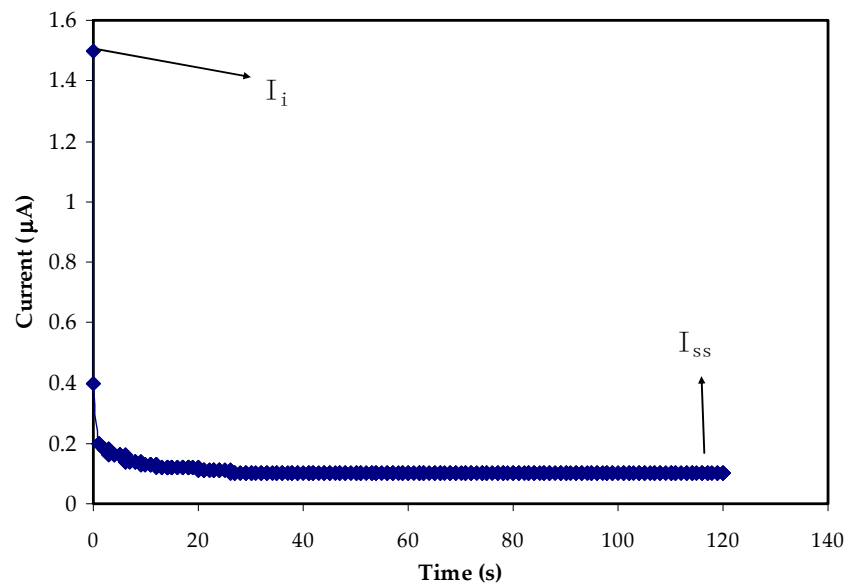
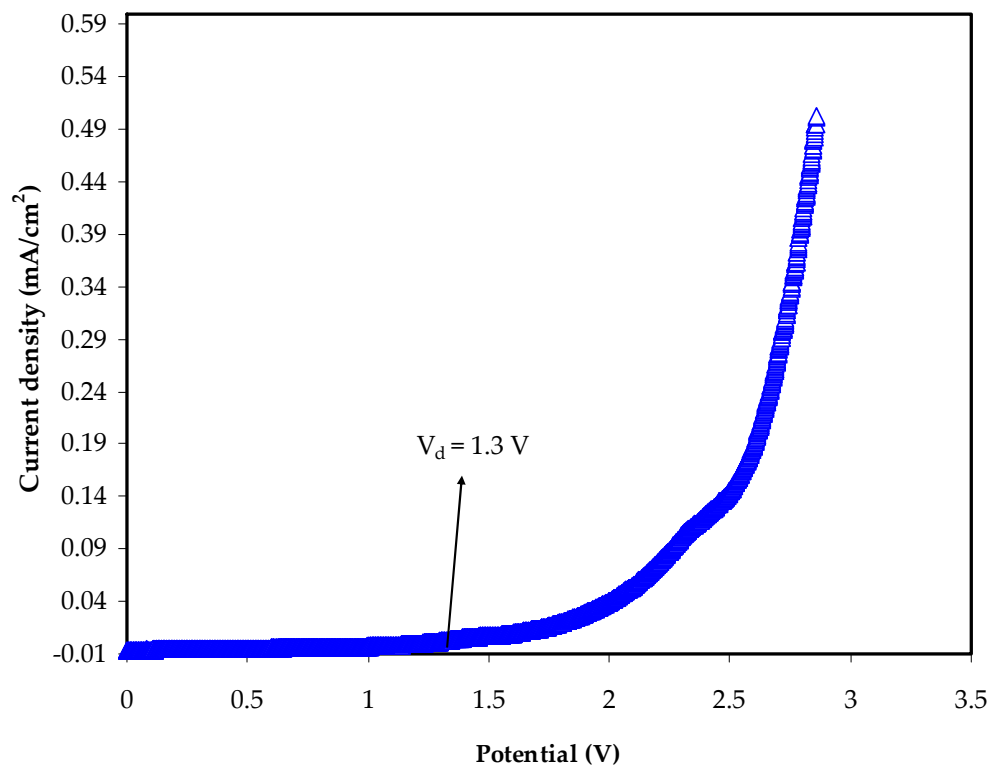**Figure 6.** Polarization of the highest conducting electrolyte at 0.2 V.

Figure 7. Linear Sweep Voltammetry (LSV) graph of the highest conducting electrolyte at 0.02 V/s.

3.5. Charge-Discharge Study

Figure 8 shows the charge-discharge cycle of the fabricated EDLC. An ideal capacitor will show a triangle curve due to polarization. Unlike conventional batteries where the discharge curve is non-linear due to the process of inter-and de-intercalation. Figure 9 shows the V_d and ESR of the EDLC in this work. V_d is energy loss and highly dependent on the internal resistance. V_d can be observed before every discharging process where the calculated average value is 0.0631 V. The value of V_d throughout the 500 cycles is quite stable at 125th and 475th cycles. This could be due to changes in ionic transportation

pattern and the formation of the charge-double layer is disturbed. In addition to that, the ESR is also stable up to 500 cycles with an average of 63.1 ohms. A low value of ESR indicates that the constituents of EDLC have an excellent contact.
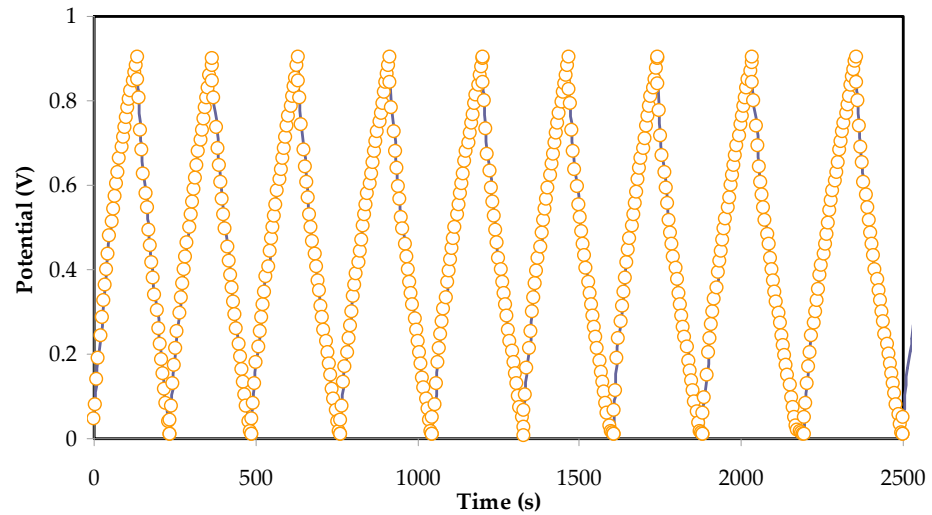

Figure 8. Selected charge–discharge graphs of the EDLC at 0.5 mA/cm^2.
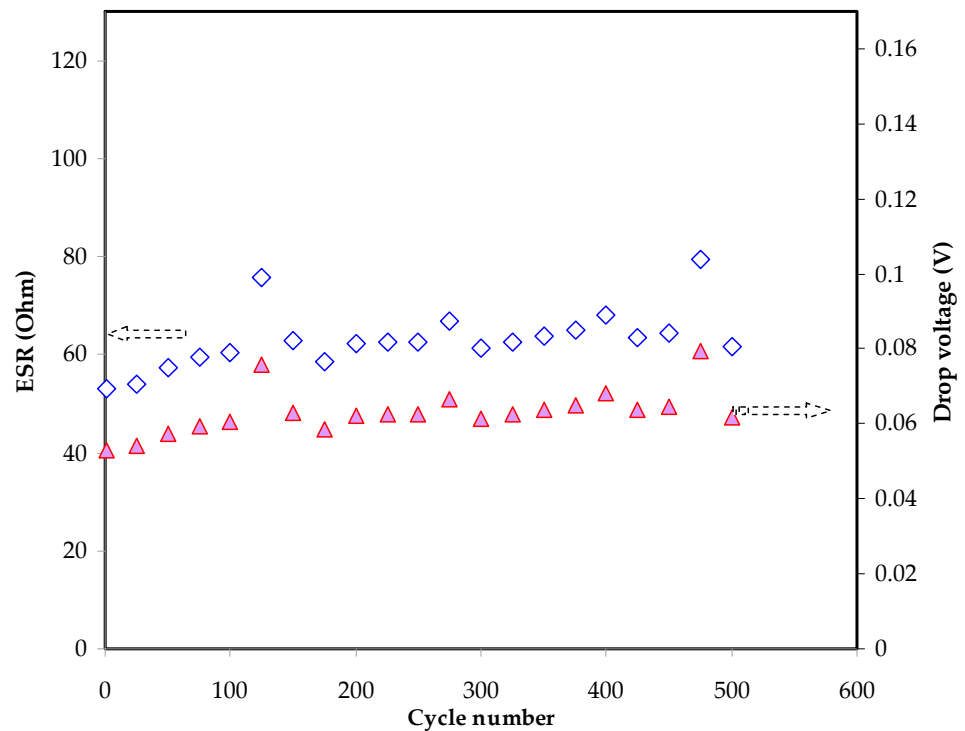

Figure 9. Equivalent series resistance (ESR) and drop voltage of the EDLC for 500 cycles of charging and discharging.

Figure 10 illustrates the C_s and efficiency as a function of cycle number for the fabricated EDLC at 0.5 mA/cm^2. The C_s value increases from 50.2 F/g at the 1st cycle to 68 F/g at the 150th cycle, followed by almost unchanging value after the 175th cycle upwards and reached an average value of 75 F/g when 500 cycles are completed. A rapid build-up of the double layers in EDLCs/supercapacitors is a main reason that the capacitance value is relatively low at the 1st cycle.
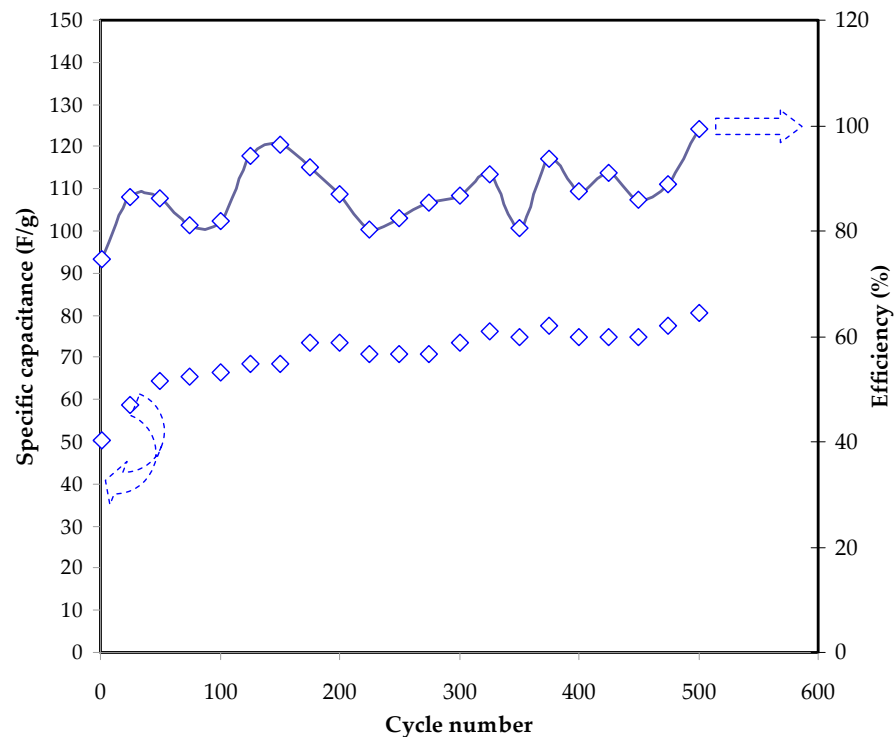
Figure 10. C_s and efficiency of the EDLC against the cycle number at 0.5 mA/cm^2.

Negatively and positively charged ions are still employed to get used to the conduction pattern at the initial stage [84,85]. Table 4 shows an example of reported works related to the application of EDLC using various types of polymer electrolytes and materials. Many aspects have to be considered such as salts, polymer, filler, plasticizer, and electrodes used.

Table 4. Various types of electrochemical double-layer capacitor (EDLC) with their relative electrodes and specific capacitance value.

System	Active Materials	C (F/g)	Reference
hydroxylethyl cellulose + MgTf$_2$ + EMIMT + silica nanoparticles	Activated carbon	25.1	[1]
PVA + CH$_3$COONH$_4$ + BmImCl	Activated carbon	31.3	[86]
MC + NH$_4$NO$_3$ + PEG	PEG/Activated carbon	38.0	[87]
PVA/polystyrene	Carbon	40.0	[88]
Cellulose + Na$_2$SO$_4$	Cellulose nanofiber + graphite	43.0	[89]
CS + MC+ NH$_4$NO$_3$ + glycerol	**Activated carbon**	**50.2**	**Present work**

The efficiency of the EDLC is illustrated in Figure 10. The high value of efficiency signifies that the discharging part is equal to or longer than the charging time. The efficiency of 74% can be observed at the first cycle. Usually, the charging process lasts longer in comparison with discharging. By subjecting the current, cations and anions begin approaching the electrode and become familiar with the conduction trend. A low efficiency is given at this stage. The efficiency is varied in the range of 80–99%. These findings of the present work reveal that the EDLC possesses good cycling stability and contact as well as less charge drop up to 500 cycles.

Figure 11 depicts the variation of *E* and *P* over 500 cycles, respectively. The *E* value was found to be 6.79 Wh/kg at the first cycle and then reached 9.52 Wh/kg. Beyond 175 cycles, E is clearly started to stabilize at an average value of 10.38 Wh/kg all over the 500 charge–discharge cycles. This fact clarifies that both NO$_3^-$ anions and NH$_4^+$ or H$^+$ cations in the polymer chains of the CS:MC blend move towards the electrode surface at an almost similar energy barrier [90]. Winie et al. [91], demonstrated that a CS-based

EDLC has energy density from 0.57 to 2.8 Wh/kg as the current density changes from 2 to 0.6 mA/cm^2, respectively. The low ion aggregation is due to stability in energy density and capacitance pattern. The EDLC shows a higher power density than batteries owing to the absence of the intercalation/deintercalation process in the former one. This needs more energy and a longer distance for ions to move back to the electrolyte. *P* value at the 1st cycle was found to be 1941 W/kg and minimized to 1633 W/kg at the 150th cycle. Yassine et al. [92], mentioned that the power density is largely linked to internal resistance; therefore, the *P* pattern will be opposed to the ESR pattern. An increase in the ESR value leads to a drop in the value of *P*. After the 175th cycle, the *P* pattern remained almost unchanged with an average value of 1642 W/kg.
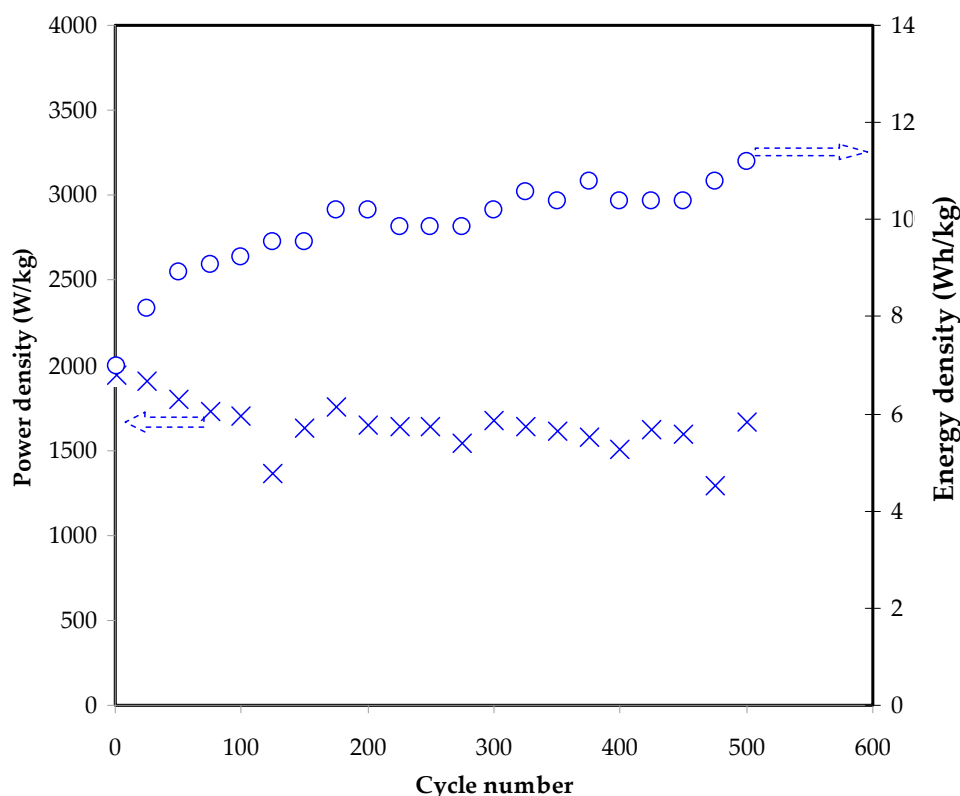

Figure 11. The plot of *E* and *P* of the EDLC versus the cycle number at 0.5 mA/cm^2.

4. Conclusions

In conclusion, structural, impedance, ion transport parameters, and device performances of the prepared electrolyte have been examined. The transport parameters and DC conductivity estimated from the EIS study reveals the suitability of the electrolyte for device fabrication. The FTIR results and their significant deconvolution were used to detect the interaction that occurs among polymer electrolyte components and determine the transport parameters. The transport properties completed from FTIR analysis is close enough to that achieved from EIS data. The dominant role of ion to the total conductivity was proven from transference number measurement (TNM) as the ionic was found to be 0.93. CS-MC-NH$_4$NO$_3$–glycerol electrolyte was potentially stable up to 1.87 V. The EDLC was tested for 500 complete charge–discharge cycles. The specific capacitance has a pattern that is similar to that of the energy density as both of them are quite related and the values are stabilized beyond 175th cycles. The specific capacitance and energy density of the EDLC at the first cycle are 50.2 F/g and 6.97 Wh/kg, respectively. Meanwhile, the internal resistance and power density of the EDLC have a similar trend. The average power density and internal resistance of the EDLC throughout the 500 cycles are 1642 W/kg

and 63.14 ohms, respectively. The performance of the EDLC can be improved by other researchers via the modifications of electrodes and electrolytes.

References

1. Chong, M.Y.; Numan, A.; Liew, C.-W.; Ng, H.M.; Ramesh, K.; Ramesh, S. Enhancing the performance of green solid-state elec-tric double-layer capacitor incorporated with fumed silica nanoparticles. *J. Phys. Chem. Solids* **2018**, *117*, 194–203. [CrossRef]
2. Ramaswamy, M.; Malayandi, T.; Selvasekarapandian, S.; Srinivasalu, J.; Rangaswamy, M.; Soundararajan, V. Development and study of solid polymer electrolyte based on polyvinyl alcohol: $Mg(ClO_4)_2$. *Polym.-Plast. Technol. Eng.* **2017**, *56*, 992–1002. [CrossRef]
3. Mustafa, M.S.; Ghareeb, H.O.; Aziz, S.B.; Brza, M.A.; Al-Zangana, S.; Hadi, J.M.; Kadir, M.F.Z. Electrochemical Characteristics of Glycerolized PEO-Based Polymer Electrolytes. *Membranes* **2020**, *10*, 116. [CrossRef]
4. Asnawi, A.S.F.M.; Hamsan, M.H.; Aziz, S.B.; Kadir, M.F.Z.; Matmin, J.; Yusof, Y.M. Impregnation of [Emim] Br ionic liquid as plasticizer in biopolymer electrolytes for EDLC application. *Electrochim. Acta* **2021**, *375*, 137923. [CrossRef]
5. Mazhandu, Z.S.; Muzenda, E.; Mamvura, T.A.; Belaid, M.; Nhubu, T. Integrated and Consolidated Review of Plastic Waste Management and Bio-Based Biodegradable Plastics: Challenges and Opportunities. *Sustainability* **2020**, *12*, 8360. [CrossRef]
6. Misenan, M.S.M.; Isa, M.I.N.; Khiar, A.S.A. Electrical and structural studies of polymer electrolyte based on chi-tosan/methyl cellulose blend doped with BMIMTFSI. *Mater. Res. Express* **2018**, *5*, 5. [CrossRef]
7. Hadi, J.M.; Aziz, S.B.; Nofal, M.M.; Hussein, S.A.; Hamsan, M.H.; Brza, M.A.; Abdulwahid, R.T.; Kadir, M.F.Z.; Woo, H.J. Electrical, Dielectric Property and Electrochemical Performances of Plasticized Silver Ion-Conducting Chitosan-Based Polymer Nanocomposites. *Membranes* **2020**, *10*, 151. [CrossRef] [PubMed]
8. Taghizadeh, M.T.; Seifi-Aghjekohal, P. Sonocatalytic degradation of 2- hydroxyethyl cellulose in the presence of some nanoparticles. *Ultrason. Sonochem.* **2015**, *26*, 265–272. [CrossRef] [PubMed]
9. Singh, P.; Bharati, C.D.; Gupta, P.N.; Saroj, A.L. Vibrational, thermal and ion transport properties of $PVA-PVP-PEG-MeSO_4Na$ based polymer blend electrolyte films. *J. Non-Cryst. Solids* **2018**, *494*, 21–30. [CrossRef]
10. Prajapati, G.; Roshan, R.; Gupta, P. Effect of plasticizer on ionic transport and dielectric properties of $PVA–H_3PO_4$ proton conducting polymeric electrolytes. *J. Phys. Chem. Solids* **2010**, *71*, 1717–1723. [CrossRef]
11. Gao, H.; Lian, K. Proton-conducting polymer electrolytes and their applications in solid supercapacitors: A review. *Royal Soc. Chem.* **2014**, *4*, 33091–33113. [CrossRef]
12. Hadi, J.M.; Aziz, S.B.; Mustafa, M.S.; Brza, M.A.; Hamsan, M.H.; Kadir, M.F.Z.; Ghareeb, H.O.; Hussein, S.A. Electrochemical Impedance study of Proton Conducting Polymer Electrolytes based on PVC Doped with Thiocyanate and Plasticized with Glycerol. *Int. J. Electrochem. Sci.* **2020**, *15*, 4671–4683. [CrossRef]
13. Kadir, M.F.Z. Characteristics of Proton Conducting PVA-Chitosan Polymer Blend Electrolytes. Ph.D. Thesis, Univeristy of Malaya, Kuala Lumpur, Malaysia, 2010. Available online: http://studentsrepo.um.edu.my/2744/ (accessed on 26 January 2021).
14. Iro, Z.S.; Subramani, C.; Dash, S.S. A Brief Review on Electrode Materials for Supercapacitor. *Int. J. Electrochem. Sci.* **2016**, *11*, 10628–10643. [CrossRef]
15. Inagaki, M.; Konno, H.; Tanaike, O. Carbon materials for electrochemical capacitors. *J. Power Sources* **2010**, *195*, 7880–7903. [CrossRef]
16. Zhang, D.; Zhang, X.; Chen, Y.; Yu, P.; Wang, C.; Ma, Y. Enhanced capacitance and rate capability of gra-phene/polypyrrole composite as electrode material for supercapacitors. *J. Power Sources* **2011**, *196*, 5990–5996. [CrossRef]
17. Pell, W.G.; Conway, B.E. Peculiarities and requirements of asymmetric capacitor devices based on combination of capacitor and battery-type electrodes. *J. Power Sources* **2004**, *136*, 334–345. [CrossRef]

18. Aziz, S.B.; Brza, M.A.; Hamsan, E.M.A.D.M.H.; Hadi, J.M.; Kadir, M.F.Z.; Abdulwahid, R.T. The Study of Electrical and Electrochemical Properties of Magnesium Ion Conducting CS: PVA Based Polymer Blend Electrolytes: Role of Lattice Energy of Magnesium Salts on EDLC Performance. *Molecules* **2020**, *25*, 4503. [CrossRef] [PubMed]

19. Kadir, M.F.Z.; Salleh, N.S.; Hamsan, M.H.; Aspanut, Z.; Majid, N.A.; Shukur, M.F. Biopolymeric electrolyte based on glycerolized methyl cellulose with NH4Br as proton source and potential application in EDLC. *Ionics* **2017**, *24*, 1651–1662. [CrossRef]

20. Kamarudin, K.H.; Hassan, M.; Isa, M.I.N. Lightweight and Flexible Solid-State EDLC based on Optimized CMC-NH₄NO₃ Solid Bio-Polymer Electrolyte. *ASM Sci. J.* **2018**, *1*, 29–36.

21. Wang, C.; Liu, T. Nori-based N, O, S, Cl co-doped carbon materials by chemical activation of ZnCl₂ for supercapacitor. *J. Alloys Compd.* **2017**, *696*, 42–50. [CrossRef]

22. Lee, D.-Y.; An, G.-H.; Ahn, H.-J. High-surface-area tofu based activated porous carbon for electrical double-layer capaci-tors. *J. Ind. Eng. Chem.* **2017**, *52*, 121–127. [CrossRef]

23. Arof, A.K.; Kufian, M.Z.; Syukur, M.F.; Aziz, M.F.; Abdelrahman, A.E.; Majid, S.R. Electrical double layer capacitor using poly(methyl methacrylate)–C4BO8Li gel polymer electrolyte and carbonaceous material from shells of matakucing (Dimo-carpuslongan) fruit. *Electrochim. Acta* **2012**, *74*, 39–45. [CrossRef]

24. Zhou, P.-W.; Li, B.-H.; Kang, F.-Y.; Zeng, Y.-Q. The development of supercapacitors from coconut-shell activated carbon. *New Carbon Mater.* **2006**, *21*, 125–131.

25. Wang, H.; Lin, J.; Shen, Z.X. Polyaniline (PANi) based electrode materials for energy storage and conversion. *J. Sci. Adv. Mater. Devices* **2016**, *1*, 225–255. [CrossRef]

26. Sequeira, C.A.; Plancha, M.J.; Araújo, L.P. Conductivity studies on solid polymer electrolytes. *J. Phys. Colloq.* **1994**, *4*, janvier1994. [CrossRef]

27. Miguel, E.R.D.S.; Aguilar, J.C.; De Gyves, J. Structural effects on metal ion migration across polymer inclusion membranes: Dependence of transport profiles on nature of active plasticizer. *J. Membr. Sci.* **2008**, *307*, 105–116. [CrossRef]

28. Hamsan, M.H.; Aziz, S.B.; Nofal, M.M.; Brza, M.A.; Abdulwahid, R.T.; Hadi, J.M.; Karim, W.O.; Kadir, M.F.Z. Characteristics of EDLC device fabricated from plasticized chitosan:MgCl₂ based polymer electrolyte. *J. Mater. Res. Technol.* **2020**, *9*, 10635–10646. [CrossRef]

29. Hadi, J.M.; Aziz, S.B.; Mustafa, M.S.; Hamsan, M.H.; Abdulwahid, R.T.; Kadir, M.F.Z.; Ghareeb, H.O. Role of nano-capacitor on dielectric constant enhancement in PEO:NH4SCN:xCeO₂ polymer nano-composites: Electrical and electrochemical properties. *J. Mater. Res. Technol.* **2020**, *9*, 9283–9294. [CrossRef]

30. Polu, A.R.; Kumar, R. AC impedance and dielectric spectroscopic studies of Mg²⁺ ion conducting PVA–PEG blended polymer electrolytes. *Bull. Mater. Sci.* **2011**, *34*, 1063–1067. [CrossRef]

31. Aziz, S.B.; Hamsan, M.H.; Brza, M.A.; Kadir, M.F.Z.; Muzakir, S.K.; Abdulwahid, R.T. Effect of glycerol on EDLC characteristics of chitosan:methylcellulose polymer blend electrolytes. *J. Mater. Res. Technol.* **2020**, *9*, 8355–8366. [CrossRef]

32. Zhang, S.; Yang, L.; Liu, Q. Impedance study on the interface of polyelectrolyte and metal sodium. *Solid State Ionics* **1995**, *76*, 127–132. [CrossRef]

33. Aziz, S.B.; Abdullah, O.G.; Rasheed, M.A.; Ahmed, H.M. Effect of High Salt Concentration (HSC) on Structural, Morphological, and Electrical Characteristics of Chitosan Based Solid Polymer Electrolytes. *Polymers* **2017**, *9*, 187. [CrossRef] [PubMed]

34. Zulkifli, A.M. Electrochemical Characteristics of Phthaloyl Chitosan Based Gel Polymer Electrolyte for Dye Sensitized Solar Cell Application. *Int. J. Electrochem. Sci.* **2020**, *15*, 7434–7447. [CrossRef]

35. Aziz, S.B.; Abidin, Z.H.Z.; Arof, A.K. Influence of silver ion reduction on electrical modulus parameters of solid polymer electrolyte based on chitosan-silver triflate electrolyte membrane. *Express Polym. Lett.* **2010**, *4*, 300–310. [CrossRef]

36. Zulkifli, A.M.; Said, N.I.A.M.; Aziz, S.B.; Dannoun, E.M.A.; Hisham, S.; Shah, S.; Abu Bakar, A.; Zainal, Z.H.; Tajuddin, H.A.; Hadi, J.M.; et al. Characteristics of Dye-Sensitized Solar Cell Assembled from Modified Chitosan-Based Gel Polymer Electrolytes Incorporated with Potassium Iodide. *Molecules* **2020**, *25*, 4115. [CrossRef]

37. Aziz, S.B.; Abdullah, R.M.; Rasheed, M.A.; Ahmed, H.M. Role of Ion Dissociation on DC Conductivity and Silver Nanoparticle Formation in PVA: AgNt Based Polymer Electrolytes: Deep Insights to Ion Transport Mechanism. *Polymers* **2017**, *9*, 338. [CrossRef]

38. Aziz, S.B.; Hamsan, M.H.; Abdullah, R.M.; Abdulwahid, R.T.; Brza, M.A.; Marif, A.S.; Kadir, M.F.Z. Protonic EDLC cell based on chitosan (CS): Methylcellulose (MC) solid polymer blend electrolytes. *Ionics* **2020**, *26*, 1829–1840. [CrossRef]

39. Aziz, S.B.; Abdullah, R.M. Crystalline and amorphous phase identification from the tanδ relaxation peaks and impedance plots in polymer blend electrolytes based on [CS:AgNt]x:PEO(x-1) (10 ≤ x ≤ 50). *Electrochim. Acta* **2018**, *285*, 30–46. [CrossRef]

40. Teo, L.P.; Buraidah, M.H.; Nor, A.F.M.; Majid, S.R. Conductivity and dielectric studies of Li₂SnO₃. *Ionics* **2012**, *18*, 655–665. [CrossRef]

41. Aziz, S.B.; Woo, T.J.; Kadir, M.; Ahmed, H.M. A conceptual review on polymer electrolytes and ion transport models. *J. Sci. Adv. Mater. Devices* **2018**, *3*, 1–17. [CrossRef]

42. Aziz, S.B.; Hamsan, M.H.; Abdullah, R.M.; Kadir, M.F.Z. A Promising Polymer Blend Electrolytes Based on Chitosan: Methyl Cellulose for EDLC Application with High Specific Capacitance and Energy Density. *Molecules* **2019**, *24*, 2503. [CrossRef] [PubMed]

43. Aziz, S.B.; Marif, R.B.; Brza, M.A.; Hamsan, M.H.; Kadir, M.F.Z. Employing of Trukhan Model to Estimate Ion Transport Parameters in PVA Based Solid Polymer Electrolyte. *Polymers* **2019**, *11*, 1694. [CrossRef] [PubMed]

44.　Awasthi, P.; Das, S. Reduced electrode polarization at electrode and analyte interface in impedance spectroscopy using carbon paste and paper. *Rev. Sci. Instrum.* **2019**, *90*, 124103. [CrossRef]

45.　Yahya, M.; Arof, A. Effect of oleic acid plasticizer on chitosan–lithium acetate solid polymer electrolytes. *Eur. Polym. J.* **2003**, *39*, 897–902. [CrossRef]

46.　Aziz, S.B.; Abidin, Z.H.Z. Ion-transport study in nanocomposite solid polymer electrolytes based on chitosan: Electrical and dielectric analysis. *J. Appl. Polym. Sci.* **2015**, *132*, 1–10. [CrossRef]

47.　Samsudin, A.S.; Isa, M.I.N. Characterization of carboxy methylcellulose doped with DTAB as new types of biopolymer electrolytes. *Bull. Mater. Sci.* **2012**, *35*, 1123–1131. [CrossRef]

48.　Brza, M.; Aziz, S.; Anuar, H.; Ali, F. Structural, ion transport parameter and electrochemical properties of plasticized polymer composite electrolyte based on PVA: A novel approach to fabricate high performance EDLC devices. *Polym. Test.* **2020**, *91*, 106813. [CrossRef]

49.　Brza, M.A.; Aziz, S.B.; Anuar, H.; Dannoun, E.M.A.; Ali, F.; Abdulwahid, R.T.; Al-Zangana, S.; Kadir, M.F. The Study of EDLC Device with High Electrochemical Performance Fabricated from Proton Ion Conducting PVA-Based Polymer Composite Electrolytes Plasticized with Glycerol. *Polymers* **2020**, *12*, 1896. [CrossRef] [PubMed]

50.　Aziz, S.B.; Marif, R.B.; Brza, M.A.; Hassan, A.N.; Ahmad, H.A.; Faidhalla, Y.A.; Kadir, M.F.Z. Structural, thermal, morphological and optical properties of PEO filled with biosynthesized Ag nanoparticles: New insights to band gap study. *Results Phys.* **2019**, *13*, 102220. [CrossRef]

51.　Saadiah, M.; Nagao, Y.; Samsudin, A. Proton (H^+) transport properties of CMC–PVA blended polymer solid electrolyte doped with NH_4NO_3. *Int. J. Hydrogen Energy* **2020**, *45*, 14880–14896. [CrossRef]

52.　Bourahla, S.; Benamara, A.A.; Moustefai, S.K. Infrared spectra of inorganic aerosols: Ab initio study of $(NH_4)_2SO_4$, NH_4NO_3, and $NaNO_3$. *Can. J. Phys.* **2014**, *92*, 216–221. [CrossRef]

53.　Ndruru, S.T.C.L.; Wahyuningrum, D.; Bundjali, B.; Arcana, I.M. Preparation and Characterization of Biopolymer Electrolyte Membranes Based on LiClO4-Complexed Methyl Cellulose as Lithium-ion Battery Separator. *J. Eng. Technol. Sci.* **2020**, *52*, 28. [CrossRef]

54.　Hafiza, M.; Isa, M. Correlation between structural, ion transport and ionic conductivity of plasticized 2-hydroxyethyl cellulose based solid biopolymer electrolyte. *J. Membr. Sci.* **2020**, *597*, 117176. [CrossRef]

55.　Aziz, S.B.; Hamsan, M.H.; Brza, M.A.; Kadir, M.F.Z.; Abdulwahid, R.T.; Ghareeb, H.O.; Woo, H.J. Fabrication of energy stor-age EDLC device based on CS:PEO polymer blend electrolytes with high Li+ ion transference number. *Results Phys.* **2019**, *15*, 102584. [CrossRef]

56.　Amran, N.N.A.; Manan, N.S.A.; Kadir, M.F.Z. The effect of $LiCF_3SO_3$ on the complexation with potato starch-chitosan blend polymer electrolytes. *Ionics* **2016**, *22*, 1647–1658. [CrossRef]

57.　Aziz, S.B.; Hamsan, M.H.; Nofal, M.M.; Karim, W.O.; Brevik, I.; Brza, M.; Abdulwahid, R.T.; Al-Zangana, S.; Kadir, M.F. Structural, Impedance and Electrochemical Characteristics of Electrical Double Layer Capacitor Devices Based on Chitosan: Dextran Biopolymer Blend Electrolytes. *Polymers* **2020**, *12*, 1411. [CrossRef] [PubMed]

58.　Shukur, M.F.; Azmi, M.S.; Zawawi, S.M.M.; Majid, N.A.; Illias, H.A.; Kadir, M.F.Z. Conductivity studies of biopolymer elec-trolytes based on chitosan incorporated with NH4Br. *Phys. Scr.* **2013**, *T157*, 1–5.

59.　Mejenom, A.A.; Hafiza, M.N.; Isa, M.I.N. X-Ray diffraction and infrared spectroscopic analysis of solid biopolymer electro-lytes based on dual blend carboxymethyl cellulose-chitosan doped with ammonium bromide. *ASM Sci. J.* **2018**, *11*, 37–46.

60.　Poy, S.Y.; Bashir, S.; Omar, F.S.; Saidi, N.M.; Farhana, N.K.; Sundararajan, V.; Ramesh, K.; Ramesh, S. Poly (1-vinylpyrrolidone-co-vinyl acetate) (PVP-co-VAc) based gel polymer electrolytes for electric double layer capacitors (EDLC). *J. Polym. Res.* **2020**, *27*, 50. [CrossRef]

61.　Pistorius, A.M.A.; DeGrip, W.J. Deconvolution as a tool to remove fringes from an FT-IR spectrum. *Vib. Spectrosc.* **2004**, *36*, 89–95. [CrossRef]

62.　Ramlli, M.A.; Bashirah, N.A.A.; Isa, M.I.N. Ionic Conductivity and Structural Analysis of 2-hyroxyethyl Cellulose Doped with Glycolic Acid Solid Biopolymer Electrolytes for Solid Proton Battery. *IOP Conf. Ser. Mater. Sci. Eng.* **2018**, *440*, 012038. [CrossRef]

63.　Kamarudin, K.H.; Isa, M.I.N. Structural and DC Ionic conductivity studies of carboxy methylcellulose doped with ammoni-um nitrate as solid polymer electrolytes. *Int. J. Phys. Sci.* **2013**, *8*, 1581–1587.

64.　Hafiza, M.; Isa, M. Solid polymer electrolyte production from 2-hydroxyethyl cellulose: Effect of ammonium nitrate composition on its structural properties. *Carbohydr. Polym.* **2017**, *165*, 123–131. [CrossRef]

65.　Ramlli, M.A.; Isa, M.I.N. Structural and Ionic Transport Properties of Protonic Conducting Solid Biopolymer Electrolytes Based on Carboxymethyl Cellulose Doped with Ammonium Fluoride. *J. Phys. Chem. B* **2016**, *120*, 11567–11573. [CrossRef] [PubMed]

66.　Rasali, N.M.J.; Nagao, Y.; Samsudin, A.S. Enhancement on amorphous phase in solid biopolymer electrolyte based alginate doped NH_4NO_3. *Ionics* **2018**, *25*, 641–654. [CrossRef]

67.　Rani, M.S.A.; Mohamed, N.S.; Isa, M.I.N. Investigation of the Ionic Conduction Mechanism in Carboxymethyl Cellu-lose/Chitosan Biopolymer Blend Electrolyte Impregnated with Ammonium Nitrate. *Int. J. Polym. Anal. Charact.* **2015**, *20*, 491–503. [CrossRef]

68.　Aniskari, N.A.B.; Mohd Isa, M.I.N. The effect of ionic charge carriers in 2-hydroxyethyl cellulose solid biopolymer electro-lytes doped glycolic acid via FTIR-deconvolution technique. *J. Sustain. Sci. Manag.* **2017**, *12*, 71–79.

69.　Ahmad, N.H.B.; Isa, M.I.N.B.M. Proton conducting solid polymer electrolytes based carboxymethyl cellulose doped ammo-nium chloride: Ionic conductivity and transport studies. *Int. J. Plast. Technol.* **2015**, *19*, 47–55. [CrossRef]

70. Samsudin, A.S.; Kuan, E.C.H.; Isa, M.I.N. Investigation of the Potential of Proton-Conducting Biopolymer Electrolytes Based Methyl Cellulose-Glycolic Acid. *Int. J. Polym. Anal. Charact.* **2011**, *16*, 477–485. [CrossRef]

71. Zainuddin, N.K.; Rasali, N.M.J.; Samsudin, A.S. Study on the effect of PEG in ionic transport for CMC-NH4Br-based solid polymer electrolyte. *Ionics* **2018**, *24*, 3039–3052. [CrossRef]

72. Nofal, M.M.; Aziz, S.B.; Hadi, J.M.; Abdulwahid, R.T.; Dannoun, E.M.A.; Marif, A.S.; Al-Zangana, S.; Zafar, Q.; Brza, M.A.; Kadir, M.F.Z. Synthesis of Porous Proton Ion Conducting Solid Polymer Blend Electrolytes Based on PVA: CS Polymers: Structural, Morphological and Electrochemical Properties. *Materials* **2020**, *13*, 4890. [CrossRef]

73. Rani, M.S.A.; Ahmad, A.; Mohamed, N.S. Influence of nano-sized fumed silica on physicochemical and electrochemical properties of cellulose derivatives-ionic liquid biopolymer electrolytes. *Ionics* **2018**, *24*, 807–814. [CrossRef]

74. Jaipal Reddy, M.; Chu, P.P. Effect of Mg^{2+} on PEO morphology and conductivity. *Solid State Ionics* **2002**, *149*, 115. [CrossRef]

75. Vijaya, N.; Selvasekarapandian, S.; Malathi, J.; Iwai, Y.; Nithya, H.; Kawamura, J. NMR study on PVP-NH4Cl based-proton con-ducting polymer electrolyte. *Indian J. Appl. Res.* **2013**, *3*, 506–510. [CrossRef]

76. Samsi, N.S.; Ali, R.M.; Zakaria, R.; Yahya, M.Z.A.; Ali, A.M.M. Electrical Properties of Ammonium Iodide Doped Cellulose Acetate Based Polymer Electrolyte. *ICGSCE* **2015**, *2014*, 331–338.

77. Jibreel, U.M.; Bhattacharya, B. Synthesis, Characterization, and Detailed Studies onPlasticizedPoly(ethyl meth-acrylate): NH4I PolymerElectrolyte. *Adv. Polym. Technol.* **2018**, *37*, 21693. [CrossRef]

78. Alia, R.M.; Haruna, N.I.; Alia, A.M.M.; Yahya, M.Z.A. Effect of ZnSDispersoid in Structural and Electrical Proper-ties of Plasticized CA-NH4I. *Phys. Procedia* **2012**, *25*, 293–298. [CrossRef]

79. Pande, G.P.; Kumar, Y.; Hashmi, S.A. Ionic liquid incorporated polymer electrolytes for supercapacitor application. *Indian J. Chem.* **2010**, *49*, 743–751. Available online: http://hdl.handle.net/123456789/9673 (accessed on 20 January 2021).

80. Sampathkumar, L.; Selvin, P.C.; Selvasekarapandian, S.; Perumal, P.; Chitra, R.; Muthukrishnan, M. Synthesis and characterization of biopolymer electrolyte based on tamarind seed polysaccharide, lithium perchlorate and ethylene carbonate for electrochemical applications. *Ionics* **2019**, *25*, 1067–1082. [CrossRef]

81. Monisha, S.; Mathavan, T.; Selvasekarapandian, S.; Benial, A.M.F.; Latha, M.P. Preparation and characterization of cellulose acetate and lithium nitrate for advanced electrochemical devices. *Ionics* **2017**, *23*, 2697–2706. [CrossRef]

82. Ng, L.; Mohamad, A. Effect of temperature on the performance of proton batteries based on chitosan–NH4NO3–EC membrane. *J. Membr. Sci.* **2008**, *325*, 653–657. [CrossRef]

83. Woo, H.J.; Liew, C.; Majid, S.R.; Arof, A.K. Poly (ε- caprolactone)-based polymer electrolyte for electrical doublelayer ca-pacitors. *High Perform. Polym.* **2014**, *26*, 637–640. [CrossRef]

84. Hadi, J.M.; Aziz, S.B.; Saeed, S.R.; Brza, M.A.; Abdulwahid, R.T.; Hamsan, M.H.; Abdullah, R.M.; Kadir, M.F.Z.; Muzakir, S.K. Investigation of Ion Transport Parameters and Electrochemical Performance of Plasticized Biocompatible Chitosan-Based Proton Conducting Polymer Composite Electrolytes. *Membranes* **2020**, *10*, 363. [CrossRef] [PubMed]

85. Aziz, S.B.; Hadi, J.M.; Dannoun, E.M.A.; Abdulwahid, R.T.; Saeed, S.R.; Marf, A.S.; Karim, W.O.; Kadir, M.F. The Study of Plasticized Amorphous Biopolymer Blend Electrolytes Based on Polyvinyl Alcohol (PVA): Chitosan with High Ion Conductivity for Energy Storage Electrical Double-Layer Capacitors (EDLC) Device Application. *Polymers* **2020**, *12*, 1938. [CrossRef] [PubMed]

86. Liew, C.-W.; Ramesh, S.; Arof, A.K. Good prospect of ionic liquid based-poly(vinyl alcohol) polymer electrolytes for su-percapacitors with excellent electrical, electrochemical and thermal properties. *Int. J. Hydrogen Energy* **2014**, *39*, 2953–2963. [CrossRef]

87. Shuhaimi, N.E.A.; Teo, L.P.; Woo, H.J.; Majid, S.R.; Arof, A.K. Electrical double-layer capacitors with plasticized polymer electrolyte based on methyl cellulose. *Polym. Bull.* **2012**, *69*, 807–826. [CrossRef]

88. Kumar, M.S.; Bhat, D.K. Polyvinyl alcohol–polystyrene sulphonic acid blend electrolyte for supercapacitor application. *Phys. B Condens. Matter* **2009**, *404*, 1143–1147. [CrossRef]

89. Andres, B.; Dahlström, C.; Blomquist, N.; Norgren, M.; Olin, H. Cellulose binders for electric double-layer capacitor electrodes: The influence of cellulose quality on electrical properties. *Mater. Des.* **2018**, *141*, 342–349. [CrossRef]

90. Shukur, M.F. Characterization of Ion Conducting Solid Biopolymer Electrolytes Based on Starch-chitosan Blend and Appli-cation in Electrochemical Devices. Ph.D. Thesis, University of Malaya, Kuala Lumpur, Malaysia, 2015.

91. Winie, T.; Jamal, A.; Saaid, F.I.; Tseng, T.-Y. Hexanoyl chitosan/ENR25 blend polymer electrolyte system for electrical dou-ble layer capacitor. *Polym. Adv. Technol.* **2018**, *30*, 1–10.

92. Yassine, M.; Fabris, D. Performance of Commercially Available Supercapacitors. *Energies* **2017**, *10*, 1340. [CrossRef]